

# Analysis of neutron diffraction spectra acquired *in situ* during stress-induced transformations in superelastic NiTi

R. Vaidyanathan<sup>a)</sup>

Department of Materials Science and Engineering, Massachusetts Institute of Technology, Cambridge, Massachusetts 02139

M. A. M. Bourke

LANSCE/MST, Los Alamos National Laboratory, Los Alamos, New Mexico 87545

D. C. Dunand<sup>b)</sup>

Department of Materials Science and Engineering, Massachusetts Institute of Technology, Cambridge, Massachusetts 02139

(Received 15 February 1999; accepted for publication 20 June 1999)

Neutron diffraction spectra were obtained during various stages of a reversible stress-induced austenite to martensite phase transformation in superelastic NiTi. This was accomplished by neutron diffraction measurements on bulk polycrystalline NiTi samples simultaneously subjected to mechanical loading. Analysis of the data was carried out using individual lattice plane (*hkl*) reflections as well as by Rietveld refinement. In the Rietveld procedure, strains in austenite were described in terms of an isotropic (*hkl* independent) and an anisotropic (*hkl* dependent) component. At higher stresses, austenite lattice plane reflections exhibited nonlinear and dissimilar elastic responses which may be attributed to the transformation. The texture evolution is significant in both austenite and martensite phases during the transformation and two approaches were used to describe this evolving texture, i.e., an ellipsoidal model due to March–Dollase and a generalized spherical-harmonic approach. The respective predictions of the phase fraction evolution as a function of applied stress were compared. A methodology is thus established to quantify the discrete phase strains, phase volume fractions, and texture during such transformations. © 1999 American Institute of Physics. [S0021-8979(99)09118-5]

## I. INTRODUCTION

Depending on stoichiometry, applied stress, and temperature, the intermetallic NiTi can exist either as a cubic (B2) austenite phase or as a monoclinic (B19') martensite phase. The transformation between these two phases is first order, displacive, athermal, and thermoelastic and can be induced by temperature and/or stress.<sup>1–3</sup> At room temperature, the stress-induced transformation of nickel-rich NiTi from austenite to martensite can result in tensile strains as high as 8%. On unloading, the martensite becomes unstable and transforms back to austenite, with a concomitant macroscopic strain recovery. This so-called superelastic or pseudoelastic effect is related to the shape-memory effect in which the transformation is induced thermally.

By recording diffraction spectra during mechanical loading, such reversible stress-induced austenite to martensite transformations can be investigated as they occur. The advantage of using neutrons over conventionally produced x rays is that the bulk behavior can be investigated in polycrystalline samples (the 50% transmission thickness in NiTi for Cu  $K\alpha$  x rays is approximately  $9\ \mu\text{m}$  as compared to about 3 cm for thermal neutrons<sup>4</sup>). From such a study, phase specific strain, texture, and volume fraction information can be ob-

tained as the cubic phase gradually transforms into the monoclinic phase on loading (and transforms back on unloading), providing fundamental mechanistic insight into the transformation.

For diffraction spectra obtained from specimens under mechanical load, shifts in positions of individual lattice plane (*hkl*) reflections can be converted to elastic strains.<sup>5</sup> Anisotropy arising from crystal geometry or strain redistribution among individual grains may lead to significantly different elastic responses between lattice planes, limiting the inferences that can be drawn from the analysis of individual peaks. One solution to this problem is to use Rietveld refinement,<sup>6</sup> which utilizes reflections from many lattice planes and can describe the average polycrystalline deformation. Furthermore, Rietveld refinement can account for variations in intensity due to changes in phase volume fractions (in multiphase materials) or to preferred orientation (texture). Two alternate formulations of the texture are applied to our data, namely a model due to March and Dollase<sup>7,8</sup> and a generalized spherical-harmonic texture formulation.<sup>9</sup>

In an earlier article,<sup>10</sup> we demonstrated for the first time the utility of neutron diffraction measurements to observe stress-induced transformations in polycrystalline superelastic NiTi. The present work augments our previous study while seeking to:

- (a) account for the evolving texture in Rietveld refinement

<sup>a)</sup>Electronic mail: rajan@mit.edu

<sup>b)</sup>Presently at: Department of Materials Science and Engineering, Northwestern University, Evanston, IL 60208.

- of diffraction spectra obtained during stress-induced austenite to martensite transformations;
- highlight the differences in predictions of phase fraction evolution using March–Dollase and generalized spherical-harmonic texture formulations;
  - observe the elastic strain response of individual lattice planes in austenite, especially as it coexists with martensite;
  - compare measured elastic strains and inferred phase fractions from individual lattice plane reflections and Rietveld refinement of neutron data from austenitic NiTi;
  - use a newly incorporated anisotropy factor within the Rietveld discrete phase strain description of austenite.

## II. EXPERIMENTAL PROCEDURES

### A. Sample fabrication

Prealloyed NiTi powders (99.9% pure, 49.4 at. % Ni, size between 44 and 177  $\mu\text{m}$ , from Special Metals Corp., NY) were blended with small quantities of nickel powders (99.9% pure, size between 44 and 177  $\mu\text{m}$ , from Special Metals Corp., NY) to give a nominal composition of 51.0 at. % Ni. The blended mixture was packed in a low carbon steel container (diameter 19.05 mm, thickness 3.18 mm, and length 127 mm and lined with a boron nitride coated nickel foil to prevent carbon contamination) and subjected to hot isostatic pressing (HIP) at 1065  $^{\circ}\text{C}$  and 100 MPa for 3 h. The resulting cylindrical NiTi billet was first electro-discharge machined into a cylindrical specimen that was 10 mm in diameter and 24 mm in length. This sample (designated hereafter as sample 1) was solutionized at 1000  $^{\circ}\text{C}$  for 1 h and oil quenched to room temperature (both in titanium-gettered flowing argon), annealed at 400  $^{\circ}\text{C}$  for 1 h in air, quenched in ice water, and tested as described below. Due to the limiting capability of the load frame, a maximum compressive stress of 625 MPa was applied on this sample. In order to obtain higher stresses and reduce uncertainties associated with the introduction of a new sample, sample 1 was further reduced by electro-discharge machining to a cylindrical sample 8 mm in diameter and 20 mm in length (designated hereafter as sample 2). Sample 2 was subjected to the same heat treatment as sample 1 and then tested as described below. Both samples had an average grain size of 20  $\mu\text{m}$  and displayed a homogeneous composition from microprobe analysis.

### B. Neutron diffraction and mechanical testing

Detailed information on the experimental setup can be found elsewhere<sup>11–13</sup> and is only summarized here. Neutron diffraction measurements were performed in “time-of-flight” mode using the neutron powder diffractometer (NPD) at the pulsed neutron source at Los Alamos Neutron Science Center (LANSCE), Los Alamos National Laboratory (LANL). The samples were loaded in uniaxial compression while neutron diffraction spectra were simultaneously collected in three scattering geometries. The loading axis formed an angle of 45 $^{\circ}$  with the incident neutron beam, allowing measurements in opposing 90 $^{\circ}$  detectors for which the scattering vector was parallel and perpendicular to the

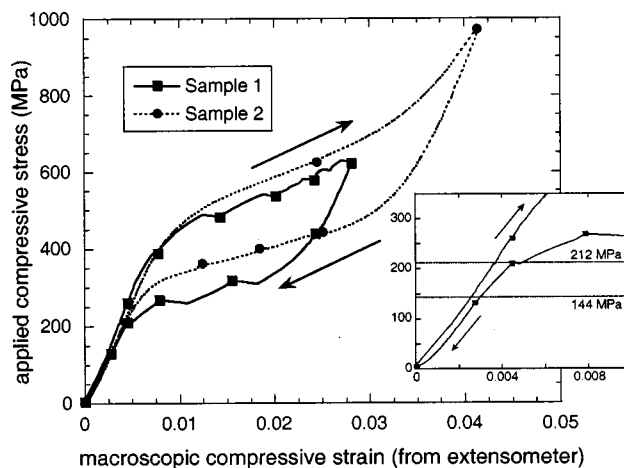


FIG. 1. Macroscopic stress-strain response of superelastic NiTi samples 1 and 2 which were tested in the neutron beam. The symbols indicate the stresses at which loading was interrupted and neutron diffraction spectra recorded. The inset shows the starting and ending regions of the transformation for sample 1.

loading axis. An additional detector in backscattering geometry at an angle of 32 $^{\circ}$  provided a third measurement. An extensometer attached to the samples recorded macroscopic strain during the experiments.

Sample 1 was uniaxially compressed to 625 MPa and then unloaded (stroke control at 3 mm/min) while sample 2, because of its reduced cross-section, was tested to 975 MPa (stroke control at 0.1 mm/min); for simplicity, compressive stress, and strain values are given as positive numbers in this article. Neutron diffraction spectra were acquired while the loading and unloading parts of the cycle were interrupted at selected stresses. Figure 1 shows the stresses and strains at which neutron spectra were obtained during loading and unloading for both samples. Both mechanical cycles were obtained after cycling the sample twice with a load-unload cycle up to 625 MPa at a stroke speed of 3 mm/min. This training procedure stabilizes the transformation by removing any initial instabilities or heterogeneities, so that the mechanical behavior observed in a trained sample is representative of the intrinsic NiTi properties.<sup>14</sup> A nonrecoverable compressive plastic strain of 0.1% was recorded after the first training cycle but none was noted after the second or the diffraction cycle. The differences in the shape of the curves of the two samples are discussed in a later section. Due to limitations in data acquisition time (approx. 6–8 h per stress level), the stresses for sample 2 were chosen to supplement data already obtained from sample 1. Diffraction data for sample 1 were the same as that obtained in our previous work.<sup>10</sup> However, in that work a complete austenite to martensite transformation was not achieved and the objective with sample 2 was to obtain a complete transformation.

### C. Transformation temperatures

Differential scanning calorimetry using a Perkin Elmer DSC-7 Calorimeter at a rate of 1 K min<sup>-1</sup> under nitrogen cover gas was used in an attempt to determine the martensite start ( $M_s$ ) and martensite finish ( $M_f$ ) temperatures for both samples. Temperatures as low as -140  $^{\circ}\text{C}$  were approached

with no observable transformation. In addition, sample 1 was cooled while neutron diffraction spectra were simultaneously obtained. A spectrum obtained at  $-253\text{ }^\circ\text{C}$  by cooling with liquid helium confirmed that the B2 austenite structure was stable to, at least, that temperature. The low temperature stability of the austenite is beyond the scope of the present publication but is discussed elsewhere.<sup>15</sup>

### III. SINGLE PEAK FITTING

By fitting individual lattice peaks, strains with respect to the unloaded state can be determined for grain orientations dictated by the specific  $hkl$  reflections. The algorithm TOFMANY<sup>16</sup> was used to fit individual lattice plane reflections in the neutron diffraction spectra. TOFMANY accounts for the inherently asymmetric peak shapes associated with the LANSCE pulsed source. Strain for a plane ( $hkl$ ) at a given stress is reported as:

$$\epsilon_{hkl} = \frac{d^{hkl} - d_0^{hkl}}{d_0^{hkl}}, \quad (1)$$

where  $d^{hkl}$  is the spacing of the plane subjected to stress and  $d_0^{hkl}$  is its spacing in the unloaded condition. In practice, a small nominal compressive stress of 8 MPa was used as the ‘‘zero stress’’ unloaded condition (this was needed to hold the specimen horizontally in the loading frame). Since the strains are calculated relative to the initial state of the specimen, the presence of pre-existing residual intergranular stresses are ignored.

Strains from individual lattice plane reflections are reported only for austenite. Martensite peaks could not be used to characterize strains because a  $d_0^{hkl}$  value for the nascent martensite cannot easily be determined and because the low-symmetry martensite has a large number of often overlapping peaks.

The simplest approach to determining the volume fraction of martensite ( $V_{\text{mar}}$ ) is from the integrated intensity of individual austenite peaks:

$$V_{\text{mar}} = 1 - V_{\text{aus}} = 1 - \left( \frac{Y_{hkl}}{Y_{hkl}^0} \right), \quad (2)$$

where the volume fraction of austenite ( $V_{\text{aus}}$ ) is determined from  $Y_{hkl}$  and  $Y_{hkl}^0$ , the integrated normalized  $hkl$  intensities at applied stress and zero stress (after training), respectively. If there is no change in texture in austenite, then each reflection should give the same volume fraction of martensite. In such a case, as austenite transforms to martensite, the austenite peak intensities would simultaneously decrease at the same rate independently of  $hkl$ . However, if the texture changes during the transformation, the corresponding changes in the peak intensities result in different  $V_{\text{mar}}$  values.

### IV. RIETVELD REFINEMENT

Instead of limiting analysis to single peaks, the Rietveld refinement method provides a mathematical model calculating the intensity,  $Y_c$ , at every point in the spectrum:

$$Y_c = Y_b + \sum_h SKF_h^2 P(\Delta T_h), \quad (3)$$

where the first term,  $Y_b$ , is the background intensity and the second term is the Bragg scattering containing a scale factor  $S$ , a correction factor  $K$ , a structure factor  $F_h$ , and a profile function  $P(\Delta T_h)$ , determined by the displacement  $\Delta T_h$  of the profile point from the reflection position. The refining procedure optimizes parameters that include phase volume fractions, atom positions, and texture until the calculated spectrum exhibits an optimum least squares fit with the measured spectrum.<sup>17</sup> The strains reported from the refinement have statistical errors about the size of the markers in the figures, i.e.,  $\pm$  half marker width. In addition, a difference curve between the measured data and refinement (as in Vaidyanathan *et al.*<sup>15</sup>) confirms the validity of the refinement. The Rietveld code General Structure Analysis System (GSAS)<sup>18</sup> was used. The profile which fitted best the data was a combination of two functions: the first is the result of convoluting two back-to-back exponentials with a Gaussian and the second is a linear combination of a Lorentzian and a Gaussian (pseudo-Voigt).

#### A. Strain description

In the current version of GSAS, the elastic strain associated with a plane,  $\epsilon_{hkl}$  is described incorporating three fitting parameters,  $\alpha$ ,  $\beta$ , and  $\gamma$ :

$$\epsilon_{hkl} = \frac{\alpha}{C} - \frac{\beta \cos \phi}{C} - \frac{\gamma A_{hkl}}{C}, \quad (4)$$

$$\frac{\alpha}{C} \equiv \epsilon_{h00}.$$

$C$  is a diffractometer constant that is used to convert time-of-flight data to  $d$  spacings.<sup>19</sup> The first fitting parameter,  $\alpha$ , fits peaks in the diffraction spectrum by varying the lattice constants  $a$ ,  $b$ , and  $c$  such that  $\Delta a/a = \Delta b/b = \Delta c/c$ . Thus  $\alpha/C$  is the strain along a nominal  $\langle h00 \rangle$  direction which is not merely determined from a  $h00$  reflection but rather from a change in the lattice constants. The second fitting parameter,  $\beta$ , accounts for the anisotropy in a given direction where  $\phi$  is the angle between  $[hkl]$  and a fixed axis, taken as  $[100]$  for the martensite. Finally, following Daymond *et al.*,<sup>20</sup> a cubic anisotropy factor,  $\gamma$ , was used to shift the position of each peak from a perfect cubic structure by a quantity proportional to  $\gamma A_{hkl}$ , where  $A_{hkl}$  is given by:

$$A_{hkl} = \frac{h^2 k^2 + h^2 l^2 + k^2 l^2}{(h^2 + k^2 + l^2)^2}. \quad (5)$$

For a cubic single crystal, the single crystal plane specific modulus,  $E_{hkl}$ , can be expressed as<sup>21</sup>

$$\frac{1}{E_{hkl}} = S_{11} - 2 \left( S_{11} - S_{12} - \frac{S_{44}}{2} \right) A_{hkl}, \quad (6)$$

where  $S_{ij}$  is the single crystal compliance tensor in collapsed matrix notation.

Only the parameters  $\alpha$  and  $\gamma$  were used to fit the cubic austenite phase. The parameter  $\beta$  was not used (i.e.,  $\beta=0$ ) so that the strain could be easily decomposed into an  $hkl$ -

independent isotropic component ( $\alpha/C$ ) and an  $hkl$ -dependent anisotropic component ( $\gamma/C$ ). Equation (4) is applicable to a cubic system but has no physical significance in quantifying the strains in the monoclinic martensite. However, strain anisotropy is observed in the martensite. Without a deterministic solution to describe this, we took the empirical approach of using all three parameters [i.e.,  $\alpha$ ,  $\beta$ , and  $\gamma$  in Eq. (4)] to better define the peak positions for the martensite. Although this invalidates any strain information for the martensite (which in any case is not reported here), we believe it does not compromise the phase fraction determination and demonstrably improves the fit of the refinement.

The preceding description applied to a refinement using spectra (with lattice plane spacings ranging from 0.6 to 4.0 Å) from all three scattering geometries. Another series of refinements were performed using only spectra (with the same lattice plane spacings range) that included reflections from all lattice planes perpendicular to the loading axis (possible since the incident beam is polychromatic). Then, only  $\alpha$  was used to describe the strain evolution in austenite and martensite, and the parameters  $\beta$  and  $\gamma$  were set to zero. The motivation in varying only  $\alpha$  was to empirically capture an "isotropic" phase strain that follows the average polycrystalline deformation since  $\epsilon_{hkl}$  would have no  $hkl$  dependence and would be the same as  $\epsilon_{h00}$  [i.e.,  $\epsilon_{hkl} = \epsilon_{h00}$  when  $\beta = \gamma = 0$  from Eq. (4)].

## B. Texture formulations

Within the correction factor  $K$  in Eq. (3) is a term which describes the change in Bragg intensity for a reflection due to texture. Two differing approaches were used. In the first, following the formulation of March and Dollase,<sup>7,8</sup> a cylindrical symmetrical version of an ellipsoidal model was used to describe the texture. Data from a single detector was analyzed using the March–Dollase formulation. The detector chosen included reflections from lattice planes perpendicular to the loading axis.

In the second, a generalized spherical-harmonic description of the orientation distribution function (which maps the probability of each of the possible grain orientations with respect to the external sample dimensions) was used. Using two sets of neutron time-of-flight data from a standard calcite sample previously used for a round-robin study, von Dreele<sup>17</sup> showed that the technique gives texture results identical with those obtained from individual reflection pole figures. Using NiTi data from all three detectors, Rietveld refinement was performed using an 8th order spherical-harmonic description.

## V. RESULTS

Figure 1 shows the macroscopic stress-strain response of superelastic NiTi samples 1 and 2 tested in the neutron beam. With increasing stress, the austenite initially deforms elastically and then progressively transforms to martensite. Sample 1 was unloaded before the transformation was complete, in contrast to sample 2, which is fully transformed and results in further elastic deformation of the transformed martensite. On unloading, the stress-induced martensite becomes

unstable and transforms back to austenite (with concurrent elastic recovery), so that all the strain is recovered.

Comparison of samples 1 and 2 in Fig. 1 shows two significant differences: (a) steps exist in the stress-strain response from sample 1 as compared to a smoother response from sample 2 and (b) the envelope of the stress-strain curves are different. The strain steps of sample 1 occur at stresses where the loading was interrupted for neutron diffraction measurements. The sample accumulated strain before reaching (within a few minutes) the stable strain levels marked with squares. This effect can be attributed to the relatively high loading rate which did not allow sufficient time for transformation enthalpy dissipation.<sup>22–24</sup> Since the transformation is thermoelastic, strain is produced when the sample equilibrates to the ambient temperature. This phenomenon occurred in the first few minutes after the load had been stabilized and thus had no significant effect on the neutron measurements which lasted about 6–8 h.

From Fig. 1 it is further observed that the stress at which martensite forms and reverts back is lower in the case of sample 1 than for sample 2. This was surprising since these two samples are physically identical (sample 2 was obtained by machining sample 1) and were subjected to the same thermomechanical treatments. However, the mechanical response of NiTi is very sensitive to temperature changes (an increase of 1 K may require an additional 4–20 MPa to initiate the transformation<sup>2</sup>). Thus the difference in mechanical behavior may be due to a slight difference in testing temperature, probably from a slightly different level of air cooling of the hydraulic equipment in the enclosed testing volume. This may have increased the ambient temperature by a few degrees for sample 2, but the temperature during the entire cycle was uniform as evidenced from the lack of steps in the stress-strain response for that sample. Recognizing this impact of testing temperature on stress, data from samples 1 and 2 have only been combined when the superelastic strain is reported. Superelastic strain refers to the total macroscopic strain measured by extensometry, from which the elastic contribution was subtracted. Unlike stress, it is a quantity characterizing the phase strains, phase fractions, and texture evolution in the transformation independently of temperature.

Figure 2 illustrates selected normalized spectra corresponding to stresses in the stress-strain curve in the inset. The evolution of the various peaks corresponding to austenite and martensite reflect the general trends in the phase evolution as a function of the applied stress. Figure 3 shows portions of the spectra corresponding to the (110) and (100) peaks of austenite at various loads. The spectra were normalized so that (110) peaks at all stresses have the same area. For clarity, the martensite reflections (where present) were subtracted from the spectra. Since each spectrum is normalized so that the (110) peak has the same area, the visible changes in the (100) peak intensity imply a change in texture in austenite. For both Figs. 2 and 3, reflections from lattice planes perpendicular to the loading axis are shown.

Figure 4 shows the volume fraction of martensite determined from the intensities of individual lattice plane reflections [using Eq. (2)] as a function of the superelastic strain

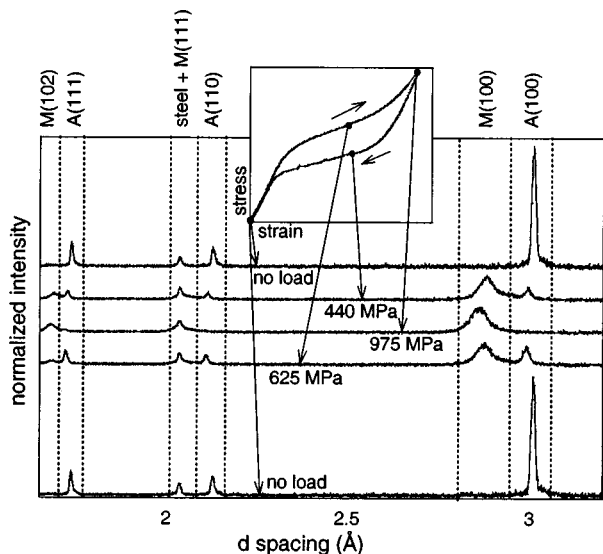


FIG. 2. Section of normalized neutron spectra from sample 2 at various stresses (see inset) showing martensite (*M*) and/or austenite (*A*) peaks. Diffraction from steel in the extensometer knife edges contaminates the *M*(111) reflection position. This did not compromise the Rietveld refinement. The reflections shown here are from lattice planes perpendicular to the loading axis.

during loading for sample 1. To determine the superelastic strain, a Young's modulus of 51 GPa, determined from a fit to the linear elastic region in the macroscopic stress-strain data for samples 1 and 2 from Fig. 1, is used. Since the macroscopic strain is much larger than the elastic strain, this elastic correction is small. The general shape of these curves in Fig. 4 is not affected even for an upper bound Young's modulus of 125 GPa, corresponding to highly textured martensite.<sup>11</sup> For clarity, only data from the relevant loading part of the cycle is shown but identical trends were observed during unloading. Figure 4 also plots the volume fractions of martensite as determined from Rietveld refinement using the March–Dollase and spherical-harmonic texture formulations.

Figure 5 illustrates the volume fraction of martensite

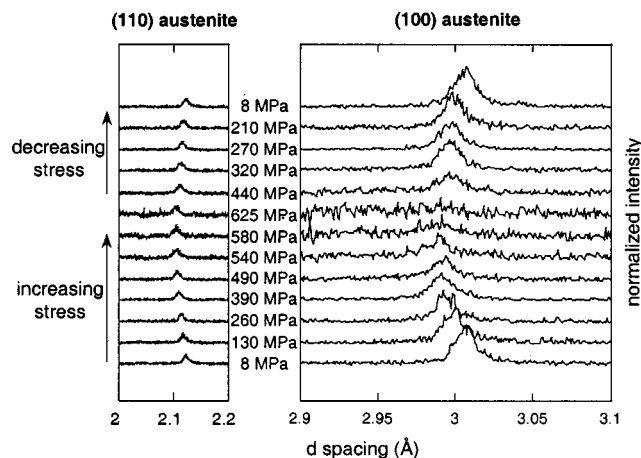


FIG. 3. The (110) and (100) peaks in austenite from sample 1 after the martensite peaks (where present) were subtracted out for clarity; the spectra were normalized so that the (110) peaks at all stresses have the same area. The reflections shown here are from lattice planes perpendicular to the loading axis.

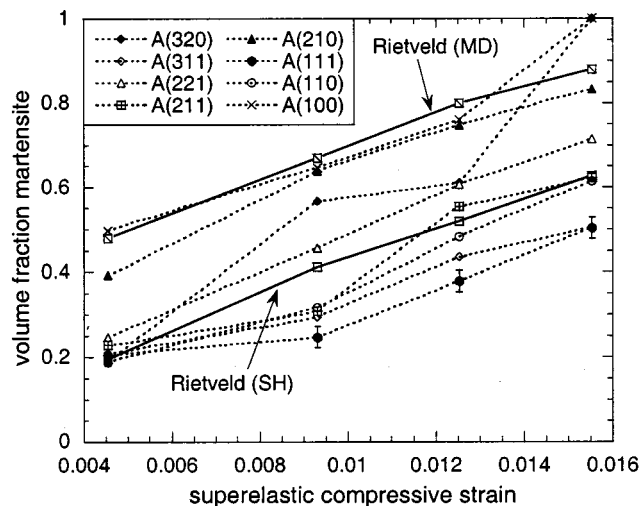


FIG. 4. Volume fraction of martensite as a function of the superelastic strain for sample 1 during loading. The volume fraction is determined from the intensities of individual austenite lattice plane reflections [using Eq. (2)] and by Rietveld refinement of the spectra using both March–Dollase (MD) and spherical-harmonic (SH) texture formulations. For clarity, typical error bars are shown only on data points from (111) reflections and are similar in magnitude for other points.

formed as a function of the superelastic strain, as determined from both March–Dollase and spherical-harmonic texture formulations. Data is included here from both samples 1 and 2 and the entire load and unload parts of the cycle. Significant qualitative and quantitative differences are noted.

As justified in the next section, the spherical-harmonic texture formulation is used in all further refinements in this work. As described earlier, two refinements were performed for each stress level using the spherical-harmonic texture formulation. In the first case only  $\alpha$  was varied for both austenite and martensite, while in the second case  $\alpha$  and  $\gamma$  were varied for austenite, and  $\alpha$ ,  $\beta$ , and  $\gamma$  for martensite [see Eq. (4)] Figures 6(a) and 6(b) show, for sample 1, strains deter-

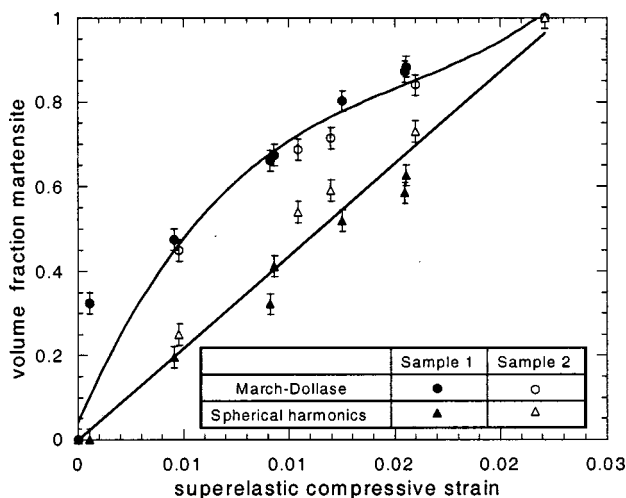


FIG. 5. Relationship between the volume fraction of martensite formed and the superelastic strain from both March–Dollase and spherical-harmonic texture formulations. Data from both the load and unload portion of the mechanical cycle are included for samples 1 and 2.

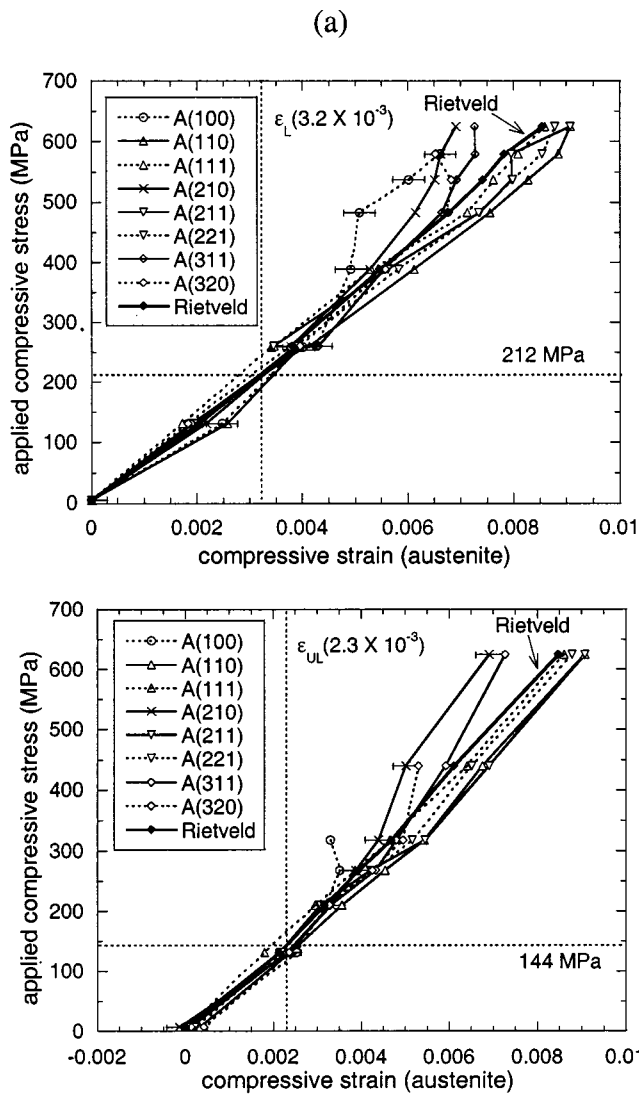


FIG. 6. The stress-strain response of individual lattice plane reflections in austenite during (a) loading and (b) unloading for sample 1 from Eq. (1). Also shown with a bold line is  $\epsilon_{h00}$  from Rietveld refinement [Eq. (4) with  $\beta = \gamma = 0$ ].  $\epsilon_L$  and  $\epsilon_{UL}$  are strains at which the anisotropy due to the transformation dominates in (a) and diminishes in (b) as determined by the  $\gamma$  parameter. For clarity, typical error bars for peak fitting are shown only on (100) in (a) and (210) in (b) and are similar in magnitude for other peaks.

mined by fitting individual peaks [Eq. (1)] in austenite as a function of the applied stress during loading and unloading. The peak reflections correspond to lattice planes perpendicular to the loading direction and hence the strains are in the direction of the applied load. Also shown is the strain obtained from Rietveld refinement where only  $\alpha$  is varied (i.e.,  $\beta = \gamma = 0$ ).

Figures 7(a) and 7(b) plot values of  $\epsilon_{h00}$  (in the set of refinements where only  $\alpha$  was varied) against  $\gamma/C$  (in the set of refinements where  $\alpha$  and  $\gamma$  were varied) for austenite during the load and unload part of the cycle for sample 1. The motivation for these plots was to observe changes in the anisotropic component of the strain in austenite as it coexists with martensite and to correlate these changes with the onset and completion of the transformation. A distinct change in

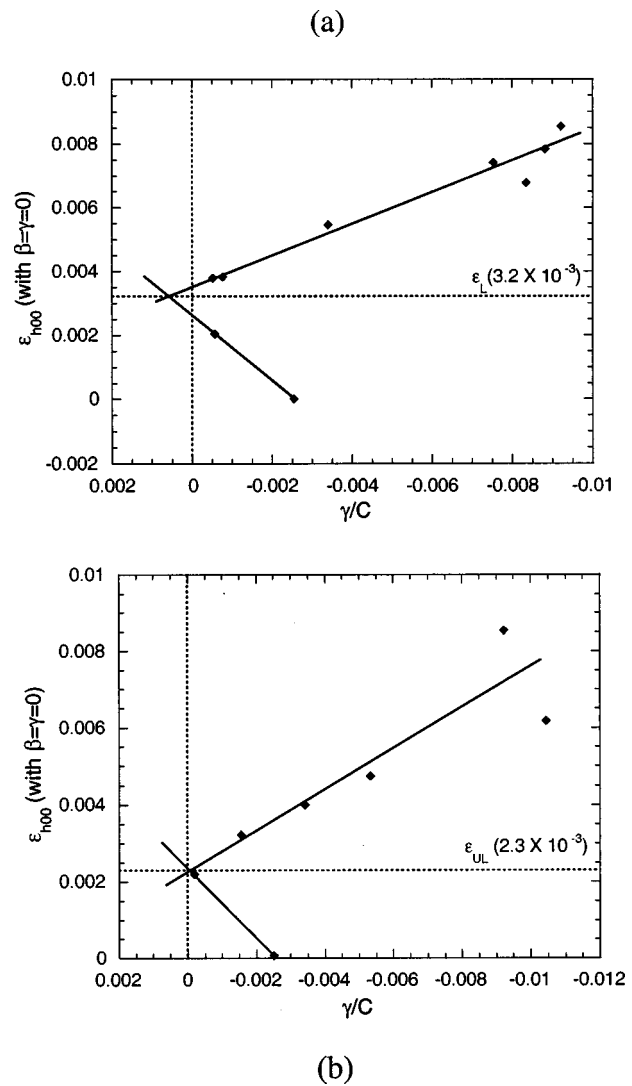


FIG. 7.  $\epsilon_{h00}$  (with  $\beta = \gamma = 0$ ) as a function of  $\gamma/C$  for austenite during (a) loading and (b) unloading for sample 1.  $\epsilon_L$  and  $\epsilon_{UL}$  are the strains [ $3.2 \times 10^{-3}$  in (a) and  $2.3 \times 10^{-3}$  in (b)] where changes in slope are observed. The diffractometer constant  $C$  is used to change  $\gamma$  time-of-flight values into strain.

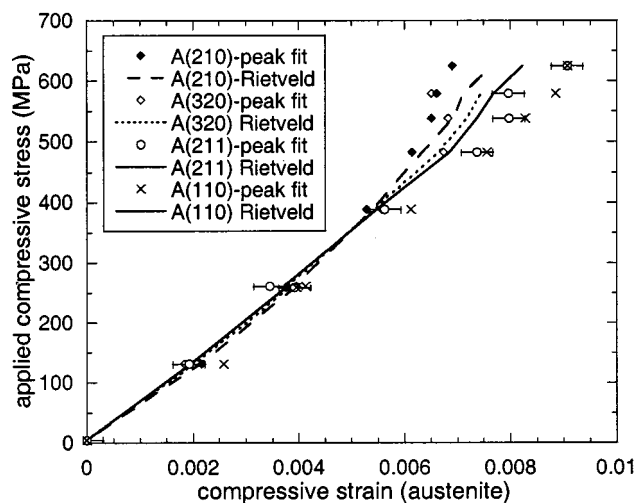
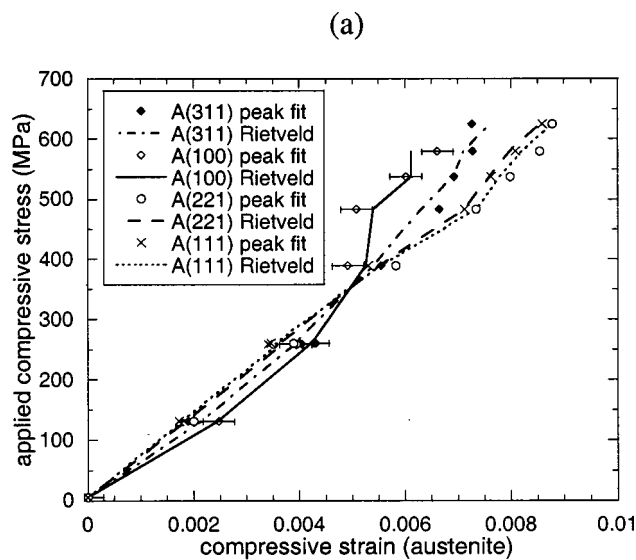
slope in these graphs is observed corresponding to changes in the anisotropic component of the strain in austenite.

Figures 8(a) and 8(b) compare the individual lattice plane strains obtained from Rietveld refinement [Eq. (4)] with those obtained by fitting single peaks [Eq. (1)] for austenite during loading in sample 1. Figures 9(a) and 9(b) are the corresponding curves during unloading in sample 1. Again, the above figures are shown for the lattice planes perpendicular to the loading direction, i.e., for strains in the direction of the applied load.

Identical trends where comparable were observed in sample 2 and have not been shown to avoid redundancy.

## VI. DISCUSSION

The stress-induced transformation from austenite to martensite and its back transformation may be inferred from the plateaus in Fig. 1. A qualitative examination of the peaks corresponding to austenite and martensite in Fig. 2, confirms

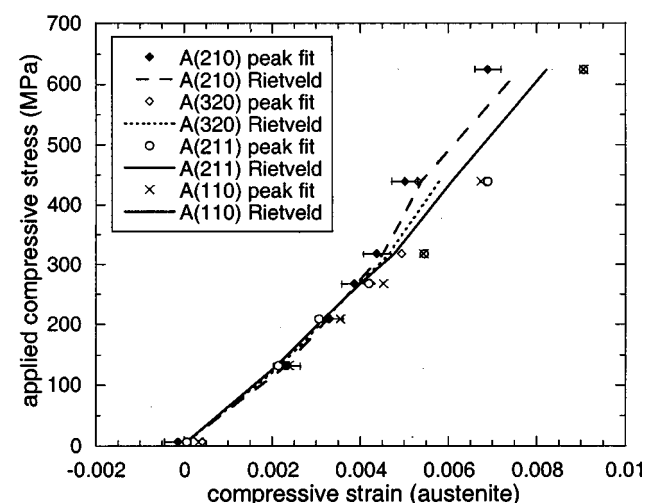
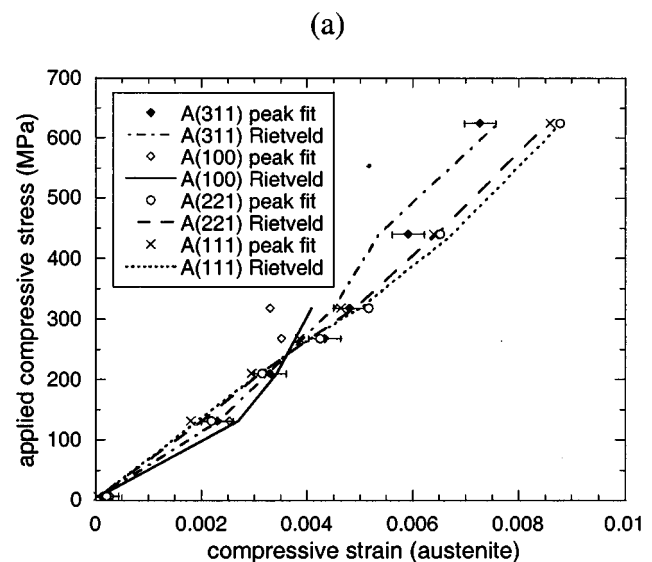


(b)

FIG. 8. Strains in individual austenite lattice planes as determined by peak fitting [Eq. (1)] and Rietveld refinement [Eq. (4)] as a function of the external applied stress during loading for sample 1. For clarity typical error bars for the peak fitting are shown only on (100) in (a) and (211) in (b) and are similar in magnitude for other peaks.

that these transformations occur within the bulk and can be observed from diffraction spectra owing to their different crystallographic structures. Our previous investigation<sup>10</sup> on sample 1 did not observe a complete transformation to martensite in contrast to the spectrum obtained at 975 MPa for sample 2.

The texture evolution in austenite is illustrated in Fig. 3 by comparing the relative intensities of (100) and (110) peaks. The austenite (100) peaks progressively decrease with respect to the (110) peaks [since each spectrum is normalized so that (110) peaks have the same area] as the load increases and austenite transforms to martensite, then revert upon unloading and back-transformation. From scattering geometry, this evolution corresponds to transformation occurring preferentially in austenite grains with their (100) planes aligned perpendicular to the loading axis, as compared to grains with their (110) planes aligned perpendicular to the load. If trans-



(b)

FIG. 9. Strains in individual austenite lattice planes as determined by peak fitting [Eq. (1)] and Rietveld refinement [Eq. (4)] as a function of the external applied stress during unloading for sample 1. For clarity typical error bars for the peak fitting are shown only on (311) in (a) and (210) in (b) and are similar in magnitude for other peaks.

formation occurs isotropically (i.e., if there was no preferential disappearance but rather a random transformation to martensite), there would be no differences in the behavior of (100) and (110) peaks. The preferential disappearance of favorably oriented grains also explains why using different peaks in Eq. (2) yields different volume fractions of martensite (Fig. 4). For example, if phase fractions are inferred from single-peak reflections alone, the (111) austenite reflection would indicate that 50 vol% martensite is present at maximum strain while the complete disappearance of the (100) austenite peaks would suggest the presence of 100% martensite. Physically, this disparity corresponds to the complete transformation of austenite grains that have their (100) planes perpendicular to the loading direction as opposed to a partial transformation of austenite grains that have their (111) planes perpendicular to the loading direction. Due to

the crystallography of the transformation, the martensite that forms is highly textured.<sup>1</sup> The unique lattice correspondence between austenite and martensite<sup>25</sup> results in austenite developing texture as well. This is analogous to developing texture by preferentially removing grains in a random sample. Detailed distributions of the evolving texture in austenite and martensite are not within the scope of this article but, along with the (11-1) type 1 twinned structure of martensite, will be discussed in another publication.<sup>26</sup> Here the emphasis is placed on accounting for the evolving texture using a formulation in Rietveld refinement that accurately determines phase fractions of martensite and austenite during the transformation.

A striking difference between the predicted phase fractions for the March–Dollase and the generalized spherical-harmonic formulations is seen in Figs. 4 and 5. The volume fraction predicted by the March–Dollase formulation is higher than that predicted by the spherical-harmonic formulation. In Fig. 4, the March–Dollase result overlaps with the most intense peaks i.e., (100) and (210), while the spherical-harmonic approach tracks a more representative behavior of the peaks. In Fig. 5, the nonlinear slope of the March–Dollase curve suggests that martensite forming at higher stress contributes more macroscopic strain than martensite forming at lower stresses. The March–Dollase prediction is unexpected since grains of austenite favorably oriented with respect to the applied stress and able to accommodate the transformation strain preferentially transform, possibly generating more strain initially or at least the same average strain.

A possible reason for the difference in predictions from the two formulations may be the strong evolving texture in martensite which leads to certain of its peaks [e.g., the (100) reflection] having very high relative intensities. The martensite (100) peak was present in spectra for which the lattice planes were perpendicular to the load, whereas it was absent in spectra for which the lattice planes were parallel to the load. Given the number of variables in Rietveld refinement and the limited amount of neutron data used (i.e., a single detector), the simple elliptical March–Dollase model overestimates the volume of martensite formed since these high intensity reflections are overweighted. This overestimation of the volume of martensite is also confirmed by a qualitative check of the diffraction spectra. In the light of the preceding discussion, the generalized spherical-harmonic description of the texture is used in further analysis of the data.

At low stresses, the stress-strain behavior observed in the different lattice planes is quite linear and similar in Figs. 6(a) and 6(b). This suggests that austenite is fairly isotropic, in agreement with ultrasonic measurements by Brill *et al.*,<sup>27</sup> who report a value of 1.94 for the anisotropy factor  $[2C_{44}/(C_{11}-C_{12})]$ , where  $C_{ij}$  is the stiffness tensor (the anisotropy factor is unity for perfect isotropy). We note again that all the lattice planes have been assumed to be stress free at the no load state in Fig. 6(a), which may not be true due to intergranular strains. To assess the plausible magnitudes of the pre-existing intergranular effects, different  $d_0^{hkl}$  values [Eq. (1)] (corresponding to different peak reflections) were used to compute lattice parameters in the unloaded state from

$d_0^{hkl}/(h^2+k^2+l^2)^{0.5}$ . The average was determined to be 3.0043 Å. By comparing the individual lattice parameters to this average lattice parameter, this simple calculation suggests that the effect of intergranular strains is largest in (100) and (110). The strain is tensile ( $9 \times 10^{-4} \pm 3 \times 10^{-4}$ ) in the case of (100) and compressive ( $6 \times 10^{-4} \pm 3 \times 10^{-4}$ ) in the case of (110), when compared to the average lattice parameter. However, these plausible residual intergranular strains are negligible compared to the elastic strain developing upon mechanical deformation.

As noted before, certain preferred orientations of austenite grains transform to martensite first. This leads to strain redistribution between grains and the elastic response of austenite lattice plane reflections are no longer linear. To satisfy compatibility between textured martensite and austenite, load transfer due to mismatch results in increasing strain anisotropy in austenite. For example the (100), (210), (320), and (311) reflections deviate significantly from a linear response to the applied stress [Figs. 6(a) and 6(b)]. Thus even though in the present case all the strain is reversible on unloading, the stress-induced austenite to martensite transformation behavior of NiTi is qualitatively similar to slip in metals in terms of the individual lattice plane responses.<sup>20,28</sup> The  $hkl$ -independent Rietveld strain  $\epsilon_{h00}$  (with only  $\alpha$  as a variable) reasonably follows the average response of the various individual lattice planes in austenite in Figs. 6(a) and 6(b).

The anisotropy in the lattice plane responses in austenite is captured in Rietveld refinement by using the  $\gamma$  parameter in Eq. (4). In Figs. 7(a) and 7(b), the  $y$  axis is a measure of the average isotropic strain in austenite ( $\epsilon_{h00}$  while only  $\alpha$  was refined and  $\beta = \gamma = 0$ ) while the  $x$  axis is a measure of the anisotropy. The absolute value of  $\gamma$  is not important, given that redefining the stress-free state (i.e., the stress-free lattice constant) of austenite can redefine the  $x$  axis. From Fig. 7(a), the anisotropy factor contribution changes slope at a strain ( $\epsilon_L$ ) of about  $3.2 \times 10^{-3}$  in austenite. This strain,  $\epsilon_L$ , represents a strain in austenite and cannot be directly compared with strain from an extensometer in NiTi (i.e., both austenite and martensite phases) because of the mechanics of load partitioning. From Fig. 6(a), an applied stress of 212 MPa corresponds to the  $\epsilon_L$  strain level in austenite. This stress is represented by the dotted line at 212 MPa in the inset in Fig. 1. The onset of the stress-induced transformation (as defined by the first deviation from linearity in the macroscopic stress-strain response in Fig. 1) occurs near this stress.

The same trend is repeated during the unload part of the cycle for sample 1 in Fig. 7(b). The hysteresis between the load and the unload part of the cycle is also captured. The stress corresponding to  $\epsilon_L = 3.2 \times 10^{-3}$  during loading is 212 MPa while the stress corresponding to  $\epsilon_{UL} = 2.3 \times 10^{-3}$  during unloading is 144 MPa, i.e., there is a difference of 68 MPa. The stress at which the anisotropy changes in the unload part of the cycle corresponds to the finish of the martensite to austenite back-transformation as shown by the dotted line at 144 MPa in the inset in Fig. 1.

To explain the anisotropy variation, we propose the following: consider the  $\gamma$  parameter as having contributions

from elasticity, plasticity associated with slip, and phase transformation, i.e.,

$$\gamma = \gamma_{el} + \gamma_{sl} + \gamma_{tran}. \quad (7)$$

The slip contribution,  $\gamma_{sl}$ , is set to zero because no slip is associated with the macroscopic stress-strain curve, as shown by the full strain recovery on unloading (Fig. 1). The elastic component of the anisotropy is always present and introduces variations in the individual lattice plane response of austenite. It is physically difficult to explain the change in slope in Figs. 7(a) and 7(b) from the  $\gamma_{el}$  contribution alone, suggesting an effect due to  $\gamma_{tran}$ . The anisotropy factor  $2C_{44}/(C_{11}-C_{12})$  for nascent, thermally formed martensite is 0.52 as reported by Brill *et al.*,<sup>27</sup> using the lattice basis of the parent austenite. The anisotropy factor in terms of the compliance elements is  $2(S_{11}-S_{12})/S_{44}$ , i.e.,  $2C_{44}/(C_{11}-C_{12})=2(S_{11}-S_{12})/S_{44}$ . Thus a change in the value of  $2C_{44}/(C_{11}-C_{12})$  from 1.94 to 0.52, corresponding to the change of a single crystal of austenite to martensite, will take  $S_{11}-S_{12}-S_{44}/2$  through a sign reversal (i.e.,  $S_{11}-S_{12}-S_{44}/2$  is greater than 0 when the anisotropy factor is greater than 1 and  $S_{11}-S_{12}-S_{44}/2$  is less than 0 when the anisotropy factor is less than 1). In Eq. (6),  $A_{hkl}$  is related to the anisotropic contribution to the modulus by  $S_{11}-S_{12}-S_{44}/2$ . This anisotropic contribution to the modulus is analogous to the anisotropic contribution to the strain in Eq. (4) with  $\gamma_{tran}$  being equivalent to  $S_{11}-S_{12}-S_{44}/2$ . Thus a sign reversal in  $S_{11}-S_{12}-S_{44}/2$  is mirrored by a sign reversal in  $\gamma_{tran}$ . This may explain the unusual anisotropic behavior observed in austenite because of its transformation to martensite. The unique lattice correspondence between austenite and martensite along with the stress and strain compatibility of austenite and martensite as they coexist may make this possible. Any real differences in the stress at which the  $\gamma$  contribution changes slope and the stress corresponding to the onset of (a) transformation or (b) dissimilar strain responses of individual lattice plane reflections can be attributed to some  $\gamma_{tran}$  contribution to  $\gamma$  canceling the  $\gamma_{el}$  contribution since they appear to act in opposite directions. The same can be expected to hold true during unloading. In a companion article,<sup>15</sup> identical behavior has been reported in a NiTi matrix transforming in the presence of TiC particles in NiTi-TiC composites.

Figures 8(a) and 8(b) compare the individual lattice plane strains obtained from Rietveld refinement [Eq. (4)] with those obtained by fitting single peaks for austenite during loading in sample 1. Such a comparison is made possible due to the introduction of  $\gamma$  in the refinement. At the lower stresses both techniques compare very well. However, there are some deviations at higher stresses especially in Fig. 8(b). The simple  $hkl$  dependence of  $\gamma$  through  $A_{hkl}$  (which is restricted to values between 0 and 1/3) was originally formulated to capture the elastic anisotropy. We have extended the same formulation to try to describe the anisotropy due to the transformation. A more rigorous relationship may result in better agreement between the two techniques. Figures 9(a) and 9(b) show the same trend during the unload part of the cycle.

While the current strain description incorporating an anisotropy factor works very well with the cubic austenite, it

remains to be seen if the fitting parameter  $\beta$  [Eq. (4)] can be used to generate some information on the monoclinic martensite. This was impossible in the present work since emphasis was placed on correctly modeling the texture and volume fraction of martensite. This was done so that convergence could be obtained in the least squares fit with Rietveld refinement. Thus  $\beta$  and  $\gamma$  served merely as fitting parameters for the monoclinic phase without any physical significance associated with it. However, it is suggested that working with very large volume fractions of martensite (>90%) and setting  $\gamma=0$  might provide some information on the use of  $\beta$  in this work.

## VII. CONCLUSIONS

Neutron diffraction measurements have been used to study the reversible stress-induced austenite to martensite transformation by obtaining diffraction data as superelastic NiTi is subjected to an uniaxial compressive stress.

- (a) The limitations associated with using a few selected peaks in the spectra to study such phase transformations are highlighted. Since the grains of austenite transform to martensite in a preferential manner, individual peak reflections do not necessarily indicate the correct volume fraction of austenite that has transformed to martensite. In addition, the stress-strain response of such reflections are not representative of the average polycrystalline deformation because of anisotropic contributions.
- (b) The texture evolves during the transformation and has to be accounted for in order to accurately quantify volume fractions of martensite and austenite during the transformation. Significant differences in predictions of phase fractions were obtained from spherical-harmonic and March-Dollase texture formulations. Comparison of the predicted phase fractions suggests that the March-Dollase model is inadequate to account for the evolving texture during such transformations.
- (c) The applied stress versus elastic strain response of individual lattice planes in austenite, while linear at lower stresses, shows significant deviation at higher stresses. This is attributed to strain redistribution on transformation to martensite.
- (d) A description of the strain that incorporates both isotropic and anisotropic components is used to quantify the elastic strain in austenite in Rietveld refinement. This strain is compared to strains obtained by fitting different single peak reflections. The isotropic component follows an average response of the various planes while addition of the anisotropic component captures the stress-strain response of the individual planes reasonably well.
- (e) The anisotropic component of the discrete phase strain description of austenite undergoes a reversal in direction in its contribution to the total strain during loading and unloading. This unusual behavior seems to correspond to the onset of the austenite to martensite trans-

formation and the conclusion of the back-transformation and may be due to the additional anisotropy introduced by the transformation.

This work has established a methodology to ascertain the discrete phase strains, phase volume fractions, and texture during stress-induced transformations to be used in investigations of the mechanics of load transfer and stress cycling in superelastic NiTi and superelastic NiTi-TiC composites.<sup>15,26,29</sup>

## ACKNOWLEDGMENTS

The Manuel Lujan Jr. Neutron Scattering Center is a national user facility funded by the United States Department of Energy, Office of Basic Energy Science and Defense Programs. This work was supported in part by DOE Contract No. W-7405-ENG-36. R. V. and D. C. D. acknowledge the support of Daimler-Benz AG, Germany in the form of a research grant and R. V.'s participation in the MIT-Germany program. The authors would like to thank Dr. M. R. Daymond, Dr. K. Bennett, and Dr. B. Von Dreele from LANSCE for helpful discussions.

<sup>1</sup>*Shape Memory Alloys*, edited by H. Funakubo (Gordon and Breach, New York, 1987).

<sup>2</sup>*Engineering Aspects of Shape Memory Alloys*, edited by T. W. Duerig, K. N. Melton, D. Stoeckel, and C. M. Wayman (Heinemann, London, 1990).

<sup>3</sup>C. M. Wayman, *MRS Bull.* **18**, 49 (1993).

<sup>4</sup>G. E. Bacon, *Neutron Diffraction* (Oxford University Press, Oxford, 1962).

<sup>5</sup>*Measurement of Residual and Applied Stress Using Neutron Diffraction*, edited by M. T. Hutchings and A. D. Krawitz (Kluwer, The Netherlands, 1992), NATO ASI Series E, No. 216.

<sup>6</sup>H. M. Rietveld, *J. Appl. Crystallogr.* **2**, 65 (1969).

<sup>7</sup>A. March, *Z. Kristallogr.* **81**, 285 (1932).

<sup>8</sup>W. A. Dollase, *J. Appl. Crystallogr.* **19**, 267 (1986).

<sup>9</sup>H. J. Bunge, *Texture Analysis in Materials Science* (Heinemann, London, 1982).

<sup>10</sup>M. A. M. Bourke, R. Vaidyanathan, and D. C. Dunand, *Appl. Phys. Lett.* **69**, 2477 (1996).

<sup>11</sup>D. C. Dunand, D. Mari, M. A. M. Bourke, and J. A. Roberts, *Metall. Mater. Trans. A* **27**, 2820 (1996).

<sup>12</sup>M. A. M. Bourke, J. A. Goldstone, and T. M. Holden, in *Measurement of Residual and Applied Stress using Neutron Diffraction*, edited by M. T. Hutchings and A. D. Krawitz (Kluwer, The Netherlands, 1992), NATO ASI Series E, No. 216, pp. 369–382.

<sup>13</sup>N. Shi, M. A. M. Bourke, J. A. Roberts, and J. E. Allison, *Metall. Mater. Trans. A* **28**, 2741 (1997).

<sup>14</sup>S. Miyazaki, T. Imai, Y. Igo, and K. Otsuka, *Metall. Trans. A* **17**, 115 (1986).

<sup>15</sup>R. Vaidyanathan, M. A. M. Bourke, and D. C. Dunand, *Acta Mater.* (in press).

<sup>16</sup>M. A. M. Bourke (personal communication).

<sup>17</sup>R. B. Von Dreele, *J. Appl. Crystallogr.* **30**, 517 (1997).

<sup>18</sup>A. C. Larson and R. B. V. Dreele, *General Structure Analysis System (GSAS)*, Report No. LAUR 8-748, Los Alamos National Laboratory (1986).

<sup>19</sup>R. B. Von Dreele, J. D. Jorgensen, and C. G. Windsor, *J. Appl. Crystallogr.* **15**, 581 (1982).

<sup>20</sup>M. R. Daymond, M. A. M. Bourke, and R. B. Von Dreele, *J. Appl. Phys.* **82**, 1554 (1997).

<sup>21</sup>J. F. Nye, *Physical Properties of Crystals* (Oxford University Press, Oxford, 1985).

<sup>22</sup>P. H. Leo, T. W. Shield, and O. P. Bruno, *Acta Metall.* **41**, 2477 (1993).

<sup>23</sup>S. Miyazaki, K. Otsuka, and Y. Suzuki, *Scr. Metall.* **15**, 287 (1981).

<sup>24</sup>P. G. McCormick and Y. Liu, *Mater. Sci. Eng., A* **167**, 51 (1993).

<sup>25</sup>T. Saburi and S. Nenno, in *Solid-Solid Phase Transformations*, edited by H. I. Aaronson, D. E. Laughlin, R. F. Sekerka, and C. M. Wayman (American Institute of Mechanical Engineers (AIME), Warrendale, Pa, 1981), pp. 1455–1479.

<sup>26</sup>R. Vaidyanathan, M. A. M. Bourke, and D. C. Dunand (unpublished).

<sup>27</sup>T. M. Brill, S. Mittelbach, W. Assmus, M. Muellner, and B. Luethi, *J. Phys.: Condens. Matter* **3**, 9621 (1991).

<sup>28</sup>B. Clausen, T. Lorentzen, and T. Leffers, *Acta Mater.* **46**, 3087 (1998).

<sup>29</sup>R. Vaidyanathan, M. A. M. Bourke, and D. C. Dunand, *Mater. Sci. Eng., A* (in print).